Compartmentalized biosynthesis of mycophenolic acid

Wei Zhang[a,b], Lei Du[a], Zepeng Qu[a,c], Xingwang Zhang[a,b], Fengwei Li[a], Zhong Li[a,c], Feifei Qi[a], Xiao Wang[a], Yuanyuan Jiang[a,c], Ping Men[a,c], Jingran Sun[a], Shaona Cao[a], Ce Geng[a], Fengxia Qi[a], Xiaobo Wan[a,d], Changning Liu[e], and Shengying Li[a,b,f,1]

[a]Shandong Provincial Key Laboratory of Synthetic Biology, Chinese Academy of Sciences (CAS) Key Laboratory of Biofuels, Qingdao Institute of Bioenergy and Bioprocess Technology, Chinese Academy of Sciences, Qingdao, 266101 Shandong, China; [b]State Key Laboratory of Microbial Technology, Shandong University, Qingdao, 266237 Shandong, China; [c]School of Life Sciences, University of Chinese Academy of Sciences, 100049 Beijing, China; [d]Key Laboratory of Optoelectronic Chemical Materials and Devices, Ministry of Education, School of Chemical & Environmental Engineering, Jianghan University, Wuhan, 430056 Hubei, China; [e]CAS Key Laboratory of Tropical Plant Resources and Sustainable Use, Xishuangbanna Tropical Botanical Garden, Chinese Academy of Sciences, Menglun, 666303 Yunnan, China; and [f]Laboratory for Marine Biology and Biotechnology, Qingdao National Laboratory for Marine Science and Technology, Qingdao, 266237 Shandong, China

Edited by Craig A. Townsend, Johns Hopkins University, Baltimore, MD, and accepted by Editorial Board Member Michael A. Marletta May 28, 2019 (received for review December 24, 2018)

Mycophenolic acid (MPA) from filamentous fungi is the first natural product antibiotic to be isolated and crystallized, and a first-line immunosuppressive drug for organ transplantations and autoimmune diseases. However, some key biosynthetic mechanisms of such an old and important molecule have remained unclear. Here, we elucidate the MPA biosynthetic pathway that features both compartmentalized enzymatic steps and unique cooperation between biosynthetic and β-oxidation catabolism machineries based on targeted gene inactivation, feeding experiments in heterologous expression hosts, enzyme functional characterization and kinetic analysis, and microscopic observation of protein subcellular localization. Besides identification of the oxygenase MpaB′ as the long-sought key enzyme responsible for the oxidative cleavage of the farnesyl side chain, we reveal the intriguing pattern of compartmentalization for the MPA biosynthetic enzymes, including the cytosolic polyketide synthase MpaC′ and *O*-methyltransferase MpaG′, the Golgi apparatus-associated prenyltransferase MpaA′, the endoplasmic reticulum-bound oxygenase MpaB′ and P450-hydrolase fusion enzyme MpaDE′, and the peroxisomal acyl-coenzyme A (CoA) hydrolase MpaH′. The whole pathway is elegantly comediated by these compartmentalized enzymes, together with the peroxisomal β-oxidation machinery. Beyond characterizing the remaining outstanding steps of the MPA biosynthetic steps, our study highlights the importance of considering subcellular contexts and the broader cellular metabolism in natural product biosynthesis.

mycophenolic acid | fungal natural product | biosynthesis | peroxisomal β-oxidation | compartmentalization

Mycophenolic acid (MPA; **1**), which was discovered from *Penicillium brevicompactum* in 1893 (1), is the first natural product antibiotic to be isolated and crystallized in human history. Today, its different active forms (e.g., CellCept by Roche, Myfortic by Novartis) have annual sales over $1 billion, owing to their wide use as first-line immunosuppressive drugs to control immunologic rejection during organ transplantations and to treat autoimmune diseases (2, 3). Mechanistically, **1** inhibits inosine-5′-monophosphate dehydrogenase; this enzyme catalyzes a known pathway-regulating step of guanine synthesis, which is essential for lymphocyte proliferation (4). This immunosuppressant is a tetraketide-terpenoid (TKTP) compound; this family comprises various chemical structures with a wide spectrum of biological activities (*SI Appendix*, Fig. S1), and TKTPs are the largest class of meroterpenoids produced by filamentous fungi (5). Despite both its status as one of the oldest natural product antibiotics and the growing number of studies reporting the characterization of fungal TKTP biosynthetic pathways (5–8), a full understanding of **1** biosynthesis has remained elusive for more than a century. This knowledge gap is especially conspicuous when one considers that the industrial fermentation of **1** has been established for decades and its structure is not particularly complex, with a full synthesis having been demonstrated by 1969 (9).

The first insights into **1** biosynthesis, which were gained more than four decades ago from culture feeding studies using synthetic radioactive isotope labeling precursors, revealed its skeleton is derived from 5-methylorsellinic acid (**2**) and farnesyl pyrophosphate (FPP), as well as a putative oxidative cleavage of the farnesyl (C_{15}) side chain (10–12). The *C*-methyl group at C6 and the *O*-methyl group at C5 were proposed to originate from *S*-adenosyl-L-methionine (SAM) (10, 13). However, the genetic and enzymological bases for **1** biosynthesis remained obscure until the recent independent discoveries of three analogous biosynthetic gene clusters of **1** (14–16) (*SI Appendix*, Fig. S2). Upon identification of these clusters, a subset of the **1** biosynthetic pathway steps has been revealed through the functional characterization of three biosynthetic enzymes: MpaC (14, 17) and MpaDE (18) from *P. brevicompactum* IBT23078 and MpaG′ from *P. brevicompactum* NRRL864 (Pb_{864}) (15) (Fig. 1).

Using examples from the *mpa′* gene cluster of Pb_{864} (*SI Appendix*, Table S1) to illustrate the present state of knowledge about **1** biosynthesis (Fig. 1), it is known that the MpaC′ enzyme

Significance

Here, we elucidate the full biosynthetic pathway of the fungal natural product mycophenolic acid (MPA). Besides the intriguing enzymatic mechanisms, we reveal that the MPA biosynthetic enzymes are elegantly compartmentalized; the oxygenase MpaB′ is the long-sought enzyme responsible for initiating the oxidative cleavage of the farnesyl side chain; and the subcellular localization of the acyl-coenzyme A hydrolase MpaH′ in peroxisomes is required for the unique cooperation between biosynthetic and β-oxidation catabolism machineries. This work highlights the importance of a cell biology perspective for understanding the underexplored organelle-associated essential catalytic mechanisms in natural product biosynthesis of fungi and other higher organisms. The insights gained in our study will benefit future efforts for both industrial strain improvement and novel drug development.

Author contributions: W.Z., L.D., and S.L. designed research; W.Z., L.D., Z.Q., X.Z., F.L., Z.L., Feifei Qi, X. Wang, Y.J., P.M., J.S., S.C., Fengxia Qi, and C.L. performed research; C.G. contributed new analytic tools; W.Z., L.D., Z.Q., X.Z., F.L., Z.L., Feifei Qi, X. Wang, Y.J., C.G., X. Wan, C.L., and S.L. analyzed data; and W.Z., X.Z., X. Wan, and S.L. wrote the paper.

The authors declare no conflict of interest.

This article is a PNAS Direct Submission. C.A.T. is a guest editor invited by the Editorial Board.

[1]To whom correspondence may be addressed. Email: lishengying@sdu.edu.cn.

This article contains supporting information online at www.pnas.org/lookup/suppl/doi:10.1073/pnas.1821932116/-/DCSupplemental.

Published online June 17, 2019.

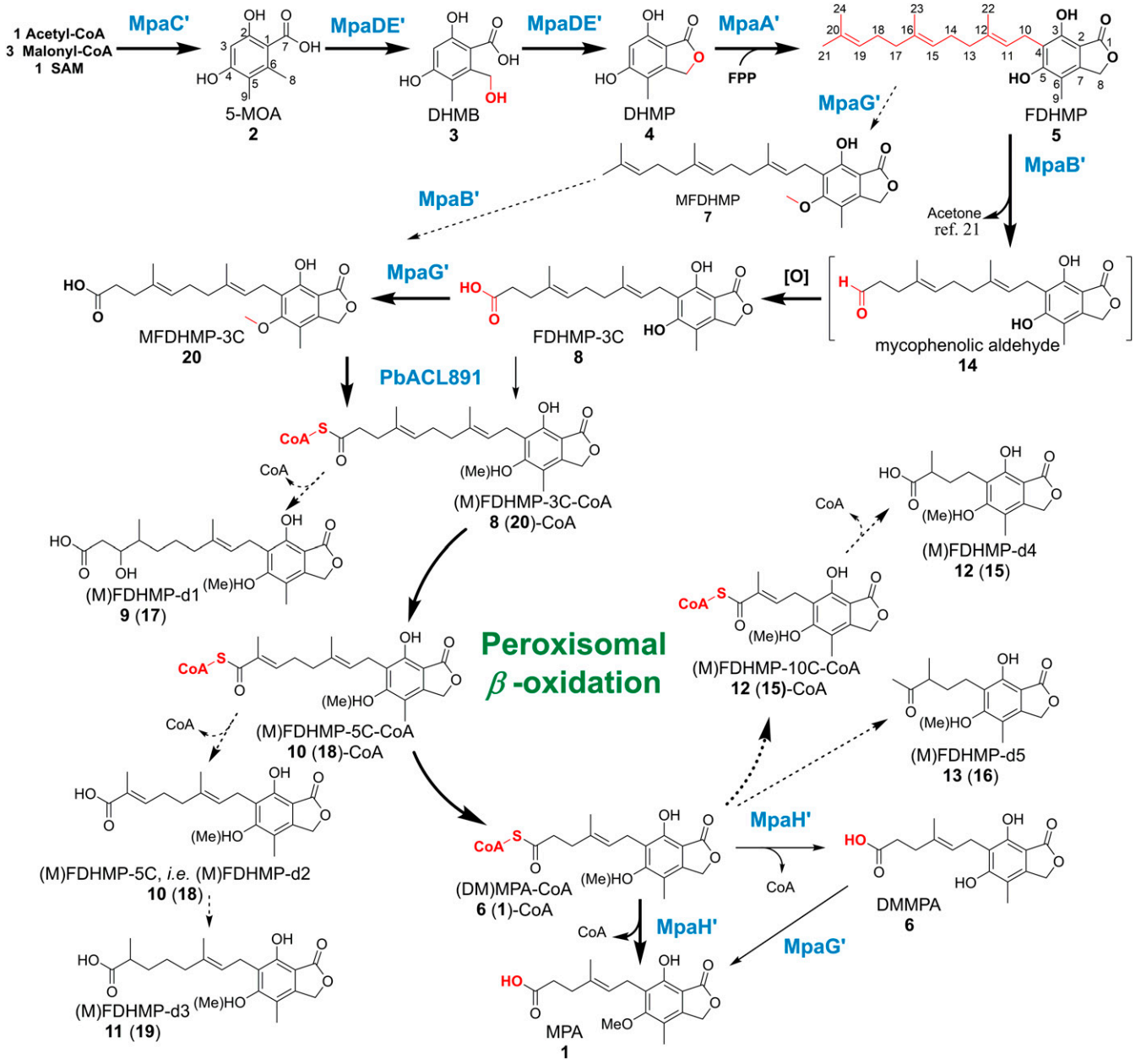

Fig. 1. MPA biosynthetic pathway. Bold solid, solid, and dashed arrows indicate the major, minor, and shunt pathways, respectively. The newly installed functional groups are colored red.

is a polyketide synthase that catalyzes the formation of **2** from one acetyl-coenzyme A (acetyl-CoA) molecule, three malonyl-CoA units, and one SAM molecule. The fascinating MpaDE′ enzyme comprises a cytochrome P450 domain (MpaD′) fused to a hydrolase domain (MpaE′) and catalyzes both the formation of 3,5-dihydroxy-7-(hydroxymethyl)-6-methylbenzoic acid (DHMB; **3**) via the C8 hydroxylation activity of MpaD′ and the subsequent intramolecular lactonization by MpaE′ to produce 3,5-dihydroxy-6-methylphthalide (DHMP; **4**). The following biosynthetic steps lack experimental confirmation, but it has been proposed that DHMP is next farnesylated by the prenyltransferase MpaA′ to yield the isolatable intermediate 4-farnesyl-3,5-dihydroxy-6-methylphthalide (FDHMP; **5**) (19–22). The biosynthetic steps between **5** and the penultimate product demethylmycophenolic acid (DMMPA; **6**) have been speculated (14, 23) but remain uncharacterized, while the final step is proposed to be the *O*-methylation of the C5 hydroxy group of **6** by the *O*-methyltransferase MpaG′ (15) to yield the final product **1**.

Results and Discussion

Our exploration of **1** biosynthesis in the present study started with our efforts to experimentally confirm that the putative prenyltransferase MpaA′ can indeed add a farnesyl group to **4** to form **5**. To prepare the hypothetical MpaA′ substrate **4**, which is commercially unavailable, we cloned the *mpaDE′* gene into the pTAex3 vector harboring the amylase promoter/terminator of P_{amyB}/T_{amyB} and the *argB* selective marker (24). The resulting pTAex3-*mpaDE′* (*SI Appendix*, Fig. S3) was used for protoplast-polyethylene glycol transformation of the popular arginine auxotrophic *Aspergillus oryzae* M-2-3 ($Ao_{M\text{-}2\text{-}3}$) (25). The maltose-induced expression of MpaDE′ in a selected PCR-confirmed fungal transformant $Ao_{M\text{-}2\text{-}3}$-*mpaDE′* (*SI Appendix*, Fig. S4 and Table S3) led to a complete conversion of the fed

synthetic **2** (20 mg/L) into **4** upon a 5-d postinduction cultivation in Czapek–Dox (CD) medium (Fig. 2 *A*, trace ii). Compound **4** was purified by semipreparative C18 reverse-phase high-performance liquid chromatography (HPLC), and its identity was confirmed by high-resolution mass spectrometry (HRMS) and NMR analyses (*SI Appendix*, Figs. S5 and S6 and Tables S4 and S5).

Next, we used $Ao_{M\text{-}2\text{-}3}$ again as the heterologous expression host to conduct in vivo assays of MpaA′ activity [note that attempts to heterologously express this transmembrane protein (*SI Appendix*, Fig. S7) in *Escherichia coli* and *Saccharomyces cerevisiae* were unsuccessful]. When **4** (20 mg/L) was fed to a maltose-induced culture of the pTAex3-*mpaA′* (*SI Appendix*, Figs. S3 and S4 and Table S2) harboring strain $Ao_{M\text{-}2\text{-}3}$-*mpaA′* (*SI Appendix*, Table S3), the precursor **4** was completely converted into a much more hydrophobic product within 5 d (Fig. 2*A*), and analysis of HRMS data showed that the molecular formula of this product was $C_{24}H_{32}O_4$ (*SI Appendix*, Fig. S8 and Table S4), which is consistent with that of the farnesylated **4**. NMR analyses of the purified compound further structurally confirmed the product as **5** (20–22) (*SI Appendix*, Figs. S9 and S10 and Table S6).

Notably, **5** was only detected in the extracts prepared from mycelia, but not the fermentation broth (Fig. 2 *A*, traces iv and vi), suggesting that **5** might have difficulty in passing through the fungal cell membrane, owing perhaps to its presumably membrane-embedded nature (like FPP) (25). Thus, MpaA′ does catalyze the transfer of a farnesyl group from FPP to **4** via C–C bond formation. However, compound **2** was not farnesylated in a similar feeding experiment (*SI Appendix*, Fig. S11), highlighting the high substrate specificity of MpaA′.

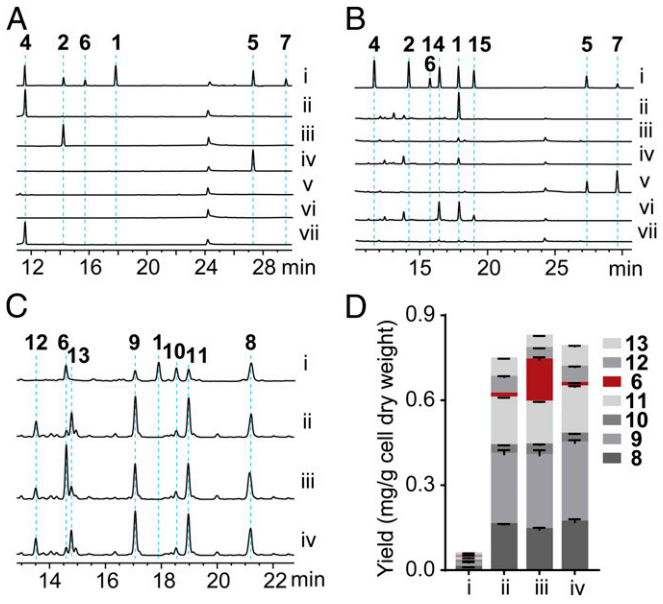

Fig. 2. HPLC analysis (254 nm) of $Ao_{M\text{-}2\text{-}3}$ precursor feeding experiments and Pb_{864} knockout mutants. (*A*) i, standards; ii, the extracellular extract of $Ao_{M\text{-}2\text{-}3}$-*mpaDE′*/**2**; iii, the extracellular extract of $Ao_{M\text{-}2\text{-}3}$-*pTAex3*/**2** as the control of ii; iv, the intracellular extract of $Ao_{M\text{-}2\text{-}3}$-*mpaA′*/**4**; v, the intracellular extract of $Ao_{M\text{-}2\text{-}3}$-*pTAex3*/**4** as the control of iv; vi, the extracellular extract of $Ao_{M\text{-}2\text{-}3}$-*mpaA′*/**4**; vii, the extracellular extract of $Ao_{M\text{-}2\text{-}3}$-*pTAex3*/**4** as the control of vi. (*B*) i, standards; ii, the extracellular extract of Pb_{864}; iii, the intracellular extract of PB_{864}; iv, the extracellular extract of Pb_{864}-*ΔmpaB′*; v, the intracellular extract of Pb_{864}-*ΔmpaB′*; vi, the extracellular extract of Pb_{864}-*ΔmpaH′*; vii, the intracellular extract of Pb_{864}-*ΔmpaH′*. (*C*) i, standards; ii, the extracellular extract of $Ao_{M\text{-}2\text{-}3}$-*mpaA′-mpaB′*/**4**; iii, the extracellular extract of $Ao_{M\text{-}2\text{-}3}$-*mpaA′-mpaB′-mpaH′*/**4**; iv, the extracellular extract of $Ao_{M\text{-}2\text{-}3}$-*mpaA′-mpaB′-mpaH′*$^{\triangle GKL}$/**4**. (*D*) Quantitative analysis of the production of **6** and the derivatives of **5**. i, $Ao_{M\text{-}2\text{-}3}$-*mpaA′*; ii, $Ao_{M\text{-}2\text{-}3}$-*mpaA′-mpaB′*; iii, $Ao_{M\text{-}2\text{-}3}$-*mpaA′-mpaB′-mpaH′*; iv, $Ao_{M\text{-}2\text{-}3}$-*mpaA′-mpaB′-mpaH′*$^{\triangle GKL}$. The amount of each compound was calculated by plotting its integrated peak area to the corresponding standard curve, and chloramphenicol was used as an internal standard.

Having experimentally confirmed the farnesyl transfer activity of MpaA′, we next attempted to unravel the long-standing biosynthetic mystery of which biomolecule(s) is responsible for the assumed oxidative cleavage of the central C_{15}=C_{16} double bond in the farnesyl chain of **5** (1, 14, 20–23). Additional genes of the *mpa′* gene cluster include *mpaF′*, *mpaB′*, and *mpaH′*; we did not pursue MpaF′ as a candidate for oxidative cleavage functionality because it is known to be an inosine-5′-monophosphate dehydrogenase involved in the self-resistance of **1**-producing strains (14, 26). To investigate the unknown functions of MpaB′ and MpaH′, we used a split-marker recombination strategy (27) to singly knock out *mpaB′* or *mpaH′* in Pb_{864} (*SI Appendix*, Fig. S12) to produce the inactivation mutants Pb_{864}-*ΔmpaB′* and Pb_{864}-*ΔmpaH′* (*SI Appendix*, Table S3).

Compared with Pb_{864} (1.58 mg/g of cell dry weight), Pb_{864}-*ΔmpaB′* produced a dramatically decreased amount (~0.12 mg/g of cell dry weight) of **1** (Fig. 2 *B*, trace iv), but this strain accumulated a significant amount of **5** in its mycelia during a 7-d cultivation using potato dextrose broth (Fig. 2 *B*, trace v). Additionally, a product was detected in the intracellular fraction of Pb_{864}-*ΔmpaB′*, whose structure was determined as 5-*O*-methyl-FDHMP (MFDHMP; **7**; Fig. 1) by HRMS (*SI Appendix*, Fig. S8 and Table S4) and NMR analyses (*SI Appendix*, Figs. S13–S17 and Table S6). We reason that the inactivation of MpaB′ blocked the normal conversion of **5**, which was methylated to **7** [likely by MpaG′ (as discussed below), which has been reported to display considerable substrate flexibility (15)]. Of note, the small amount of **1** produced by Pb_{864}-*ΔmpaB′* (Fig. 2*B*, trace iv) suggests the existence of minor compensating enzymatic activity for MpaB′ in Pb_{864}.

To further elucidate the functionality of MpaB′, **5** (20 mg/L) was fed to an induction culture of $Ao_{M\text{-}2\text{-}3}$-*mpaB′* (*SI Appendix*, Table S3). Surprisingly, no obvious products were detected (*SI Appendix*, Fig. S18). We reason that this negative result might be due to the difficulty for **5** to enter the intracellular space, which is supported by our earlier observation that **5** was not secreted outside of $Ao_{M\text{-}2\text{-}3}$-*mpaA′* cells (Fig. 2*A*). To overcome this issue, the recombinant strain $Ao_{M\text{-}2\text{-}3}$-*mpaA′-mpaB′* was generated and cultured in CD medium supplemented with maltose to induce the coexpression of MpaA′ and MpaB′ for 3 d, to which **4** (20 mg/L) was added. Upon an additional 5-d cultivation, an intermediate with three fewer carbon atoms than **5** was observed (Fig. 2 *C*, trace ii), purified, and structurally identified as FDHMP-3C (**8**; Fig. 1 and *SI Appendix*, Figs. S8 and S19–S23 and Tables S4 and S7). Interestingly, **8** was previously proposed as a putative intermediate *en route* to **1** (12, 21) (*SI Appendix*, Fig. S24).

We also found that $Ao_{M\text{-}2\text{-}3}$-*mpaA′-mpaB′* produced additional derivatives with ultraviolet absorption spectra similar to those of **5** and **8** (Fig. 2 *C*, trace ii), which presumably derived from **5**; these were therefore deemed FDHMP-d1–d5 (**9**–**13**). Structural determination (*SI Appendix*, Figs. S8 and S25–S39 and Tables S4, S7, and S8) showed that these derivatives appear to be chain-shortening intermediates of **8** that also bear some additional modifications, suggesting a possible biodegradation pathway through which **8** may undergo a β-oxidation process in which a C_2/C_3 unit can be successively lost over repeated rounds (Fig. 1). Of note, it was previously reported that branched-chain fatty acids can be degraded via a β-oxidation process (28, 29). Strikingly, a small amount of **6** was also detected, giving an initial hint that *mpaH′* may not be a required gene for **6** production.

These results collectively establish that it is MpaB′ which functions as an oxygenase to mediate the oxidative cleavage of the C_{19}=C_{20} double bond in **5** to yield **8**. Recall that there are no reports of any known function for MpaB′, and we did not identify any obvious functional domains using BLAST or Pfam database tools. However, when using the Phyre2 program (30) to predict and compare potentially conserved three-dimensional structural features with other proteins, we noted a possible similarity in a structural fold with a distant homolog (11%/22% amino acid identity/similarity; *SI Appendix*, Figs. S40 and S41): a *b*-type

heme-containing protein from *Streptomyces* sp. K30 (Lcp_{K30}) that was recently biochemically and structurally characterized as a latex-clearing enzyme (31, 32).

Consideration of the proposed catalytic mechanisms from the Lcp_{K30} study (32) guided our speculation that MpaB′ might initiate the oxidative cleavage through hydrogen atom abstraction by D124 at the C_{18} allylic position. The resultant iron(IV)-oxo species could then react with the epoxide, together with a D124-mediated acid–base catalysis, ultimately leading to the cleavage of the C_{19}=C_{20} double bond (32) (*SI Appendix*, Fig. S42). The expected resultant aldehyde was not observed, likely owing to instability; supporting this, chemically synthesized mycophenolic aldehyde (**14**; *SI Appendix*, Fig. S43 and Table S4) was readily oxidized to **1** by $Ao_{M\text{-}2\text{-}3}$ (*SI Appendix*, Fig. S44). Thus, our results overturn the previously proposed direct cleavage of the C_{15}=C_{16} double bond of **5** (10–12) (*SI Appendix*, Fig. S24), which would otherwise lead to **6** but not the observed **8** and other intermediates (**9**–**11**) that are longer than **6**, as the dominant product when $Ao_{M\text{-}2\text{-}3}$-*mpaA′*-*mpaB′* was fed with **4** (Fig. 2 *C*, trace ii).

Next, HPLC analysis of the fermentation culture of an aforementioned Pb_{864}-Δ*mpaH′* strain led to the surprising finding that this *mpaH′* knockout strain retained the ability to produce **1** (Fig. 2 *B*, trace vi), albeit with a yield (~0.75 mg/g of dry cell weight) that was ~50% lower than that of Pb_{864} (Fig. 2 *B*, trace ii). This mutant strain also produced two compounds [MFDHMP-d4 (**15**) and MFDHMP-d5 (**16**)] with an even shorter isoprenyl chain than **1** (Fig. 1 and *SI Appendix*, Figs. S8 and S45–S51 and Tables S4 and S9); these correspond to the 5-*O*-methylated products of **12** and **13**, presumably stemming from the activity of MpaG′. Notably, neither compound was detected in Pb_{864} cultures by HPLC analysis (Fig. 2*B*). The attenuated production of **1**, together with the two over-shortening products by Pb_{864}-Δ*mpaH′*, suggested an interesting possibility that while MpaH′ does not catalyze the oxidative cleavage of **5** as previously proposed (14), this enzyme apparently does have an MPA biosynthesis-related function, likely somehow involved in the aforementioned β-oxidation chain-shortening process. Specifically, MpaH′ may function to control the specificity and efficiency of final production of **1**, perhaps by acting as a "valve" to prevent the excessive β-oxidation–mediated shortening of **1**.

To recapitulate the MPA accumulation pattern of Pb_{864} in a heterologous host, we investigated the product profile of the $Ao_{M\text{-}2\text{-}3}$-*mpaA′*-*mpaB′*-*mpaH′* strain (in which the three genes were coexpressed) when **4** (20 mg/L) was fed to its induction cultures. As expected, the amount of the penultimate pathway intermediate **6** that accumulated in $Ao_{M\text{-}2\text{-}3}$-*mpaA′*-*mpaB′*-*mpaH′* was significantly higher than that of $Ao_{M\text{-}2\text{-}3}$-*mpaA′*-*mpaB′* (Fig. 2 *C*, traces ii and iii, and *D*), again emphasizing the importance of MpaH′ for efficient production of either **6** or **1**. Notably, whereas we were expecting to only detect the accumulation of **6** by $Ao_{M\text{-}2\text{-}3}$-*mpaA′*-*mpaB′*-*mpaH′* as the dominant production of **1** by Pb_{864}, we were surprised to observe substantial amounts of **9**–**11** as well as low levels of **12** and **13**; note that the methylated counterparts MFDHMP-d1–d5 (**15**–**19**) were only detected at negligible levels by liquid chromatography-mass spectrometry (LC-MS) in Pb_{864}. We speculate that these differences between *Penicillium* and *Aspergillus* species could perhaps be due to their different cellular contexts. Specifically, $Ao_{M\text{-}2\text{-}3}$ may contain a nonspecific acyl-CoA hydrolase with broad and highly efficient hydrolytic activities toward the CoA esters generated from the β-oxidation catabolic pathway (*SI Appendix*, Fig. S52). The low-level accumulation of **12** and **13** likely resulted from the lower activity of MpaH′ toward DMMPA-CoA (**6**-CoA) than toward MPA-CoA (**1**-CoA), which could lead to the "leaking" of these two excessively chain-shortened derivatives from peroxisomes (as discussed below). Nonetheless, our observation of **9**–**13** represented important clues for our following elucidation of the unusual **1** biosynthetic pathway steps.

Interestingly, a PSORT II (33) analysis of the MpaH′ sequence identified a type 1 peroxisomal targeting sequence-like (PTS1-like) glycine-lysine-leucine (GKL) tripeptide at its C terminus, which strongly suggested that this protein is localized in peroxisomes, a site where β-oxidation metabolism can occur (34, 35). We were able to successfully confirm the peroxisomal localization of MpaH′ via confocal laser scanning microscopy (CLSM) of several *Aspergillus* strains expressing GFP fusion constructs for full-length and GKL-tripeptide–truncated MpaH′ variants alongside the recombinant expression of the peroxisome-specific RFP^{SKL} reporter (*SI Appendix*, Tables S2 and S3). As anticipated, we observed colocalization of the RFP^{SKL} reporter with the GFP-$MpaH'^{full\text{-}length}$, but not the GFP-$MpaH'^{\Delta GKL}$, fusion protein (Fig. 3 *A*–*D* and *SI Appendix*, Fig. S53). Additionally, feeding experiments demonstrated that the peroxisomal localization of MpaH′ increases the efficiency of **6** production; specifically, a significantly higher amount of **6** accumulated in the **4**-fed $Ao_{M\text{-}2\text{-}3}$-*mpaA′*-*mpaB′*-*mpaH′* cultures than in the corresponding $Ao_{M\text{-}2\text{-}3}$-*mpaA′*-*mpaB′*-$mpaH'^{\Delta GKL}$ cultures (Fig. 2 *C*, traces iii and iv, and *D*).

In line with our proposed "valve" function of the peroxisomal protein MpaH′, the fact that fungal β-oxidation of long-chain acyl moieties can occur in peroxisomes (34, 36), together with our observation of the suspected β-oxidation–derived chain-shortening products in the Pb_{864}-Δ*mpaH′*, $Ao_{M\text{-}2\text{-}3}$-*mpaA′*-*mpaB′*/**4** cultures (Fig. 2), and also in the culture of wild-type Pb_{864} by LC-HRMS (*SI Appendix*, Fig. S54), we hypothesized that the α/β-hydrolase fold containing MpaH′ enzyme may be an acyl-CoA hydrolase that can specifically recognize the CoA esters **6**-CoA and/or **1**-CoA. To test this, we heterologously expressed MpaH′ in *E. coli* BL21(DE3) cells and purified it to homogeneity (*SI Appendix*, Fig. S55). Indeed, when the purified MpaH′ was incubated with chemically synthesized **6**-CoA and **1**-CoA in vitro, both **6** and **1** were rapidly hydrolyzed from their corresponding CoA esters (*SI Appendix*, Fig. S56). Analysis using Phyre2 revealed a likely structural relationship between MpaH′ and the

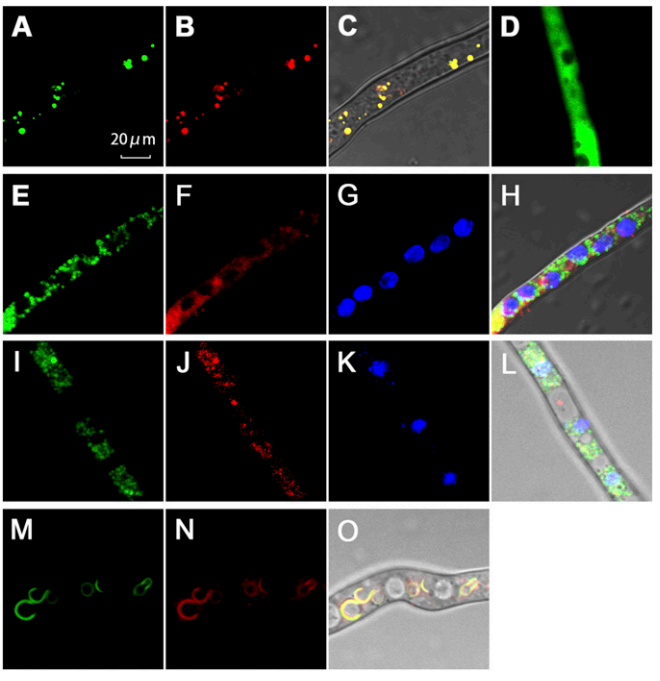

Fig. 3. High-resolution confocal images for subcellular localization of MpaH′, MpaB′, MpaDE′, and MpaA′ in $Ao_{M\text{-}2\text{-}3}$. (*A*) GFP-MpaH′ localization. (*B*) Peroxisomal localization of RFP^{SKL}. (*C*) Merged images of *A* and *B* in bright field. (*D*) GFP-$MpaH'^{\Delta GKL}$ localization. (*E*) MpaB′-GFP localization. (*F*) Localization of ER by ER-Tracker Red. (*G*) Localization of multiple nuclei by DAPI. (*H*) Merged images of *E*–*G* in bright field. (*I*) MpaDE′-GFP localization. (*J*) Localization of ER by ER-Tracker Red. (*K*) Localization of multiple nuclei by DAPI. (*L*) Merged images of *I*–*K* in bright field. (*M*) GFP-MpaA′ localization. (*N*) Localization of Golgi complex with CellLight Golgi-RFP. (*O*) Merged images of *M* and *N* in bright field. (Magnification: 20 μm.)

peroxisomal hydrolase Lpx1 from *S. cerevisiae* (35), and careful protein sequence analysis (*SI Appendix*, Fig. S57) suggested that MpaH′ is a member of the type I acyl-CoA thioesterase enzyme family. MpaH′ possesses a well-recognized catalytic triad of S139-D163-H365 (37). To confirm that S139 is the catalytic nucleophile, we mutated this serine into an alanine and, as expected, the hydrolytic activity of the MpaH′^{S139A} mutant for either **1**-CoA or **6**-CoA was completely abolished (*SI Appendix*, Fig. S56).

We subsequently analyzed the steady-state kinetics of MpaH′ in vitro using the 5,5-dithiobis-(2-nitrobenzoic acid) reagent (38) and found that the catalytic constant (k_{cat})/Michaelis constant (K_m) values of MpaH′ for both **6**-CoA (11.6 $\mu M^{-1}\cdot min^{-1}$) and **1**-CoA (81.5 $\mu M^{-1}\cdot min^{-1}$) were two orders of magnitude higher than the values for the 10 other unnatural CoA esters that we tested in similar assays (*SI Appendix*, Fig. S58 and Table S10). Thus, our results strongly suggest that MpaH′ is a dedicated acyl-CoA hydrolase with high substrate specificity toward **1**-CoA, and this enzyme apparently exerts a valve-like function to prevent **1**-CoA from further peroxisomal β-oxidation and to avoid the hydrolysis of other CoA esters.

The 6.2-fold higher k_{cat}/K_m values of **1**-CoA relative to **6**-CoA suggests (*SI Appendix*, Table S10) that the 5-*O*-methylation mediated by the methyltransferase MpaG′ likely occurs before the entry of **8** into peroxisomes. Supporting this, **8** was found to be a better substrate for MpaG′ compared with other potential substrates, including **6**, **5**, **2**, and **4** (*SI Appendix*, Fig. S59). However, we cannot exclude the possibility that methylation of **6** could also occur in vivo as a minor pathway (Figs. 1 and 4). After the cytosolic methylation of **8**, the entry of MFDHMP-3C (**20**) into peroxisomes could be unidirectional: This entry likely occurs via free diffusion due to its low molecular weight of 388, which is lower than the reported 400-Da cutoff for crossing the single membrane of peroxisome via free diffusion (34). Upon a peroxisomal CoA ligation reaction, presumably catalyzed by a β-oxidation component enzyme acyl-CoA ligase, MFDHMP-3C-CoA (**20**-CoA) with a molecular weight of 1,136 would then be restricted to peroxisomes for the following β-oxidation pathway steps (Fig. 1 and *SI Appendix*, Fig. S52).

To identify this pivotal acyl-CoA ligase (presumably a long-chain fatty acid acyl-CoA ligase considering the chain length of **20**), we searched the whole-genome sequences of Pb_{864} and found nine potential genes for long-chain fatty acid acyl-CoA ligases. To narrow down the candidate enzymes, we attempted to find some clues from *S. cerevisiae*, since this yeast is a model system for the study of β-oxidation metabolism (39), by assuming that its peroxisomal β-oxidation machinery can also process **8** as Pb_{864} and $Ao_{M\text{-}2\text{-}3}$. As predicted, a number of low-level but indicative β-oxidation intermediates were detected by LC-HRMS when **8** was fed to the culture of *S. cerevisiae* American Type Culture Collection strain 204508 for 7 d, including the transΔ^2-enoyl product **21**, the hydroxyacyl product **22**, the diketoacyl intermediate **23**, and the following chain-shortening product **10** (*SI Appendix*, Fig. S60). It is well known that *S. cerevisiae* has four long-chain fatty acid acyl-CoA ligases, FAA1–FAA4, with only FAA2 being located in the peroxisome (39). Thus, we used the FAA2-encoding sequence as a probe to blast the genome of Pb_{864}. As a result, a homologous acyl-CoA ligase gene, *PbACL891* (*SI Appendix*, Fig. S61), was discovered from Pb_{864}. Then, the recombinant *N*-His_6–tagged PbACL891 was successfully expressed in *E. coli* BL21(DE3) and purified to homogeneity (*SI Appendix*, Fig. S62). In the presence of **8**, ATP, CoA, and Mg^{2+}, this enzyme efficiently converted **8** to **8**-CoA (*SI Appendix*, Fig. S63). Thus, PbACL891, a presumable peroxisomal enzyme with a C-terminal PTS1-like alanine-lysine-leucine (AKL) tripeptide (36), is responsible for bridging the biosynthetic pathway and the peroxisomal β-oxidation process for efficient and specific production of **1**.

The importance of the subcellular localization of MpaH′ and the fact that MpaA′, MpaB′, and MpaDE′ are predicted to be membrane-associated proteins (*SI Appendix*, Figs. S7 and S64) led us to further investigate the compartmentalization of these biosynthetic enzymes. Specifically, we fused GFP tags to the N or C termini of the transmembrane MpaA′ and the integral monotopic proteins MpaB′ and MpaDE′ (*SI Appendix*, Figs. S3 and S4 and Tables S2 and S3). Subsequent CLSM observations that revealed the colocalization of the green fluorescence signals of MpaDE′-GFP (or MpaB′-GFP) and the red fluorescence signals of the "ER-Tracker Red" marker, outside of DAPI-stained nuclei, together demonstrated that both of these two proteins reside at the endoplasmic reticulum (ER) (Fig. 3 *E–L*). The green fluorescence signals of the GFP-MpaA′ fusion protein were distributed as ring-like structures in hyphal cells that were colocalized with the red fluorescence signals of the CellLight Golgi-RFP BacMam 2.0 marker that specifically targets the Golgi complex (Fig. 3 *M–O*).

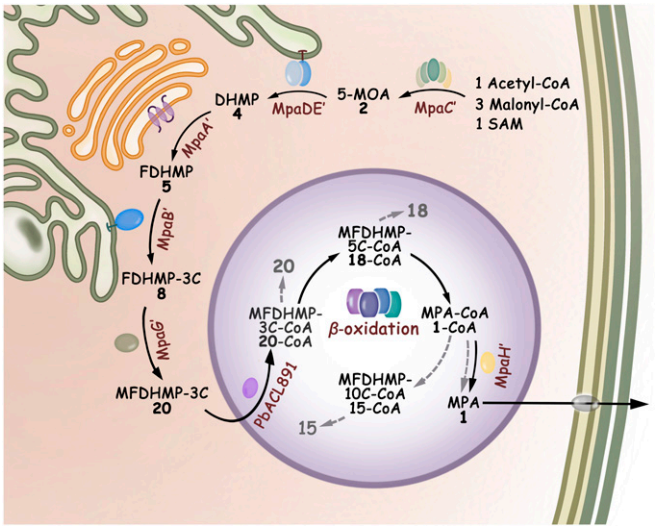

Fig. 4. Schematic compartmentalized MPA biosynthesis (solid arrows indicate the major pathway, and dashed arrows indicate the shunt pathways), which is sequentially mediated by the cytosolic polyketide synthase MpaC′, the ER-bound P450-hydrolase fusion enzyme MpaDE′, the Golgi apparatus-associated prenyltransferase MpaA′, the ER-bound oxygenase MpaB′, the cytosolic *O*-methyltransferase MpaG′, and the long-chain fatty acid acyl-CoA ligase PbACL891, the β-oxidation machinery, and the acyl-CoA hydrolase MpaH′ in peroxisomes.

The ER-bound nature of MpaDE′ is unsurprising, since membrane anchoring is a common feature of eukaryotic P450 enzymes (18). For MpaA′ and MpaB′, their membrane association is potentially functionally relevant because these enzymes must ostensibly interact with their membrane-embedded substrates, including FPP and **5**. Finally, it is worth noting that the biotransformation activities of all of the engineered strains carrying the GFP-tagged enzymes did not differ from their non-tagged counterparts, indicating that the fusion fluorescence tags did not alter the catalytic properties of these enzymes.

Conclusions

In this study, we elucidate the previously unknown steps of the full biosynthetic pathway of MPA. We envision that the insights gained in our work will benefit future efforts for both industrial strain improvement and novel drug development. The intriguing compartmentalization of the biosynthetic enzymes for **1** (Fig. 4), including the cytosolic MpaC′ and MpaG′; the inner membrane-associated MpaA′, MpaB′, and MpaDE′; and the peroxisomal acyl-CoA hydrolase MpaH′ and acyl-CoA ligase PbACL891, work together, and thus enable a unique joining of biosynthetic and β-oxidation catabolic machineries. These findings highlight that the underexplored organelle-associated catalytic mechanisms such as, for example, the final peroxisomal maturation steps of penicillin (40), can enable essential steps in natural product biosynthesis in fungi and other higher organisms. Compared with the better understanding of compartmentalization in biosynthesis of lipids (41), plant terpenoids (42), and lichen polyketides (43), the compartmentalized biosynthesis of

fungal natural products demands much more attention in the future since only very limited knowledge about the subcellular localization of fungal biosynthetic enzymes and their involvement in product formation and intermediate trafficking has been acquired so far. Finally, we suggest that studies of natural product biosynthesis should be liberated from a reductionist emphasis on enzymatic steps and would profit by adopting a more panoramic view of catalytic mechanisms, enzyme subcellular distribution, and global cellular metabolisms.

Methods

In Vitro Enzymatic Assay of MpaH′. The standard assay containing 10 nM MpaH′ and 1 mM substrate in 100 μL of reaction buffer [50 mM NaH_2PO_4 (pH 8.0), 10% glycerol] was performed at 28 °C for 20 min and quenched with an equal volume of ethyl acetate. The two-time organic extracts were combined and dried by N_2 flow, and then redissolved in 100 μL of methanol for HPLC and LC-MS analysis.

Confocal Microscopy. The transformant bearing GFP or RFP fusion constructs was grown for 3–5 d at 28 °C in CMP medium (CD medium supplemented with 3% maltose for induction and 1% peptone, 100 mL) to induce protein expression under the α-amylase promoter in a 250-mL Erlenmeyer flask. The fresh mycelia were transferred to the staining regents after washing with sterilized water three times. Specifically, 200 μL of CellLight Golgi-RFP was added to the washed mycelia and treated at 4 °C for 30 min, to which 1 mL of sterilized water was added, and the mixture was incubated at 37 °C for another 30 min. For ER-Tracker Red staining, 200 μL of regent was added to the washed mycelia and treated at 37 °C for 45 min before washing with 1 mL of sterilized water twice; after ER-Tracker Red staining, the mycelia were transferred to 150 μL of DAPI solution (800 $\mu g \cdot mL^{-1}$) for another 2 min and washed with 1 mL of sterilized water twice. Confocal laser scanning fluorescence images of fungal structures were recorded on an Olympus FluoView FV1000 laser scanning microscope (Olympus America). A krypton-argon laser was used as the source of excitation at 488 nm. The green fluorescence signals, the red fluorescence signals, and the DAPI fluorescence signals were recorded at 505 nm, 559 nm, and 619 nm, respectively. The images were processed with Olympus FluoViewVersion 4.0b.

ACKNOWLEDGMENTS. We thank Prof. Ikuro Abe (University of Tokyo), Prof. Shuangjiang Liu (Institute of Microbiology, Chinese Academy of Sciences), and Prof. Chunxiang Fu [Qingdao Institute of Bioenergy and Bioprocess Technology, Chinese Academy of Sciences (QIBEBT-CAS)] for providing the plasmids pTAex3, pAcGFP1, and pANIC 6D, respectively. We also thank Prof. Jianghua Chen (Xishuangbanna Tropical Botanical Garden, Chinese Academy of Sciences) and Prof. Guochang Sun (Zhejiang Academy of Agricultural Sciences) for helpful discussions. Moreover, we thank Drs. Jingyao Qu and Zhifeng Li (Shandong University) as well as Ms. Ying Yang and Fali Bai (QIBEBT-CAS) for their kind help in allowing us to use the LC-MS and NMR facilities. This work was supported by the National Natural Science Foundation of China (Grants 21472204 and 81741155 to S.L., Grant 31570030 to W.Z., and Grant 31600036 to Feifei Qi); the Shandong Provincial Natural Science Foundation (Grant ZR2017ZB0207 to W.Z. and S.L.); a Qilu Youth Scholar Startup Funding of Shandong University grant (to W.Z.); the Chinese Academy of Sciences (Grant QYZDB-SSW-SMC042 to S.L. and Youth Innovation Promotion Association of CAS Grant 2015166 to W.Z.); the National Postdoctoral Innovative Talent Support Program (Grant BX20180325 to L.D.); and the China Postdoctoral Science Foundation (Grants 2016T90650 and 2015M58060 to W.Z. and Grant 6188229 to F.L.).

1. R. Bentley, Mycophenolic acid: A one hundred year odyssey from antibiotic to immunosuppressant. *Chem. Rev.* **100**, 3801–3826 (2000).
2. A. V. Marzano, F. Dassoni, R. Caputo, Treatment of refractory blistering autoimmune diseases with mycophenolic acid. *J. Dermatolog. Treat.* **17**, 370–376 (2006).
3. B. C. de Winter, T. van Gelder, Therapeutic drug monitoring for mycophenolic acid in patients with autoimmune diseases. *Nephrol. Dial. Transplant.* **23**, 3386–3388 (2008).
4. C. A. Jonsson, H. Carlsten, Mycophenolic acid inhibits inosine 5′-monophosphate dehydrogenase and suppresses immunoglobulin and cytokine production of B cells. *Int. Immunopharmacol.* **3**, 31–37 (2003).
5. R. Geris, T. J. Simpson, Meroterpenoids produced by fungi. *Nat. Prod. Rep.* **26**, 1063–1094 (2009).
6. T. Mori *et al*., Molecular basis for the unusual ring reconstruction in fungal meroterpenoid biogenesis. *Nat. Chem. Biol.* **13**, 1066–1073 (2017).
7. Y. Matsuda, T. Iwabuchi, T. Wakimoto, T. Awakawa, I. Abe, Uncovering the unusual D-ring construction in terretonin biosynthesis by collaboration of a multifunctional cytochrome P450 and a unique isomerase. *J. Am. Chem. Soc.* **137**, 3393–3401 (2015).
8. Y. Matsuda, I. Abe, Biosynthesis of fungal meroterpenoids. *Nat. Prod. Rep.* **33**, 26–53 (2016).
9. A. J. Birch, J. J. Wright, A total synthesis of mycophenolic acid. *Aust. J. Chem.* **22**, 2635–2644 (1969).
10. L. Canonica *et al*., Biosynthesis of mycophenolic acid. *J. Chem. Soc. Perkin Trans. I* **21**, 2639–2643 (1972).
11. W. L. Muth, C. H. Nash, 3rd, Biosynthesis of mycophenolic acid: Purification and characterization of S-adenosyl-L-methionine: Demethylmycophenolic acid *O*-methyltransferase. *Antimicrob. Agents Chemother.* **8**, 321–327 (1975).
12. C. P. Nulton, J. D. Naworal, I. M. Campbell, E. W. Grotzinger, A combined radiogas chromatograph/mass spectrometer detects intermediates in mycophenolic acid biosynthesis. *Anal. Biochem.* **75**, 219–233 (1976).
13. L. Canonica, W. Kroszczy, B. M. Ranzi, B. Rindone, C. Scolasti, Biosynthesis of mycophenolic acid. *J. Chem. Soc. Chem. Commun.*, 1357 (1970).
14. T. B. Regueira *et al*., Molecular basis for mycophenolic acid biosynthesis in *Penicillium brevicompactum*. *Appl. Environ. Microbiol.* **77**, 3035–3043 (2011).
15. W. Zhang *et al*., Functional characterization of MpaG′, the *O*-methyltransferase involved in the biosynthesis of mycophenolic acid. *ChemBioChem* **16**, 565–569 (2015).
16. A. Del-Cid *et al*., Identification and functional analysis of the mycophenolic acid gene cluster of *Penicillium roqueforti*. *PLoS One* **11**, e0147047 (2016).
17. B. G. Hansen *et al*., Versatile enzyme expression and characterization system for *Aspergillus nidulans*, with the *Penicillium brevicompactum* polyketide synthase gene from the mycophenolic acid gene cluster as a test case. *Appl. Environ. Microbiol.* **77**, 3044–3051 (2011).
18. B. G. Hansen *et al*., Involvement of a natural fusion of a cytochrome P450 and a hydrolase in mycophenolic acid biosynthesis. *Appl. Environ. Microbiol.* **78**, 4908–4913 (2012).
19. L. Canonica, W. Kroszczy, B. M. Ranzi, B. Rindone, C. Scolasti, Biosynthesis of mycophenolic acid. *J. Chem. Soc. Chem. Commun.*, 257 (1971).
20. L. Colombo, C. Gennari, C. Scolastico Biosynthesis of mycophenolic acid. Oxidation of 6-farnesyl-5,7-dihydroxy-4-methylphthalide in a cell-free preparation from *Penicillium-brevicompactum*. *J. Chem. Soc. Chem. Commun.*, 434 (1978).
21. C. P. Nulton, I. M. Campbell, Labelled acetone and levulinic acid are formed when [^{14}C]acetate is being converted to mycophenolic acid in *Penicillium brevicompactum*. *Can. J. Microbiol.* **24**, 199–201 (1978).
22. L. Colombo, C. Gennari, D. Potenza, C. Scolastico, F. Aragozzini, (E,E)-10-(1,3-dihydro-4,6-dihydroxy-7-methyl-3-oxoisobenzofuran-5-yl)-4,8-dimethyldeca-4,8-dienoic acid: Total synthesis and role in mycophenolic acid biosynthesis. *J. Chem. Soc. Chem. Commun.*, 1021–1022 (1979).
23. R. Schor, R. Cox, Classic fungal natural products in the genomic age: The molecular legacy of Harold Raistrick. *Nat. Prod. Rep.* **35**, 230–256 (2018).
24. S. Tada *et al*., Identification of the promoter region of the Taka-amylase A gene required for starch induction. *Agric. Biol. Chem.* **55**, 1939–1941 (1991).
25. T. Itoh *et al*., Reconstitution of a fungal meroterpenoid biosynthesis reveals the involvement of a novel family of terpene cyclases. *Nat. Chem.* **2**, 858–864 (2010).
26. B. G. Hansen *et al*., A new class of IMP dehydrogenase with a role in self-resistance of mycophenolic acid producing fungi. *BMC Microbiol.* **11**, 202–206 (2011).
27. R. S. Goswami, Targeted gene replacement in fungi using a split-marker approach. *Methods Mol. Biol.* **835**, 255–269 (2012).
28. G. Vanhove *et al*., Mitochondrial and peroxisomal beta oxidation of the branched chain fatty acid 2-methylpalmitate in rat liver. *J. Biol. Chem.* **266**, 24670–24675 (1991).
29. N. M. Verhoeven *et al*., Phytanic acid and pristanic acid are oxidized by sequential peroxisomal and mitochondrial reactions in cultured fibroblasts. *J. Lipid Res.* **39**, 66–74 (1998).
30. L. A. Kelley, S. Mezulis, C. M. Yates, M. N. Wass, M. J. Sternberg, The Phyre2 web portal for protein modeling, prediction and analysis. *Nat. Protoc.* **10**, 845–858 (2015).
31. W. Röther, S. Austen, J. Birke, D. Jendrossek, Cleavage of rubber by the latex clearing protein (Lcp) of *Streptomyces* sp strain K30: Molecular insights. *Appl. Environ. Microbiol.* **82**, 6593–6602 (2016).
32. L. Ilcu *et al*., Structural and functional analysis of latex clearing protein (Lcp) provides insight into the enzymatic cleavage of rubber. *Sci. Rep.* **7**, 6179–6089 (2017).
33. K. Nakai, P. Horton, PSORT: A program for detecting sorting signals in proteins and predicting their subcellular localization. *Trends Biochem. Sci.* **24**, 34–36 (1999).
34. T. Stehlik, B. Sandrock, J. Ast, J. Freitag, Fungal peroxisomes as biosynthetic organelles. *Curr. Opin. Microbiol.* **22**, 8–14 (2014).
35. S. Thoms, J. Hofhuis, C. Thöing, J. Gärtner, H. H. Niemann, The unusual extended C-terminal helix of the peroxisomal α/β-hydrolase Lpx1 is involved in dimer contacts but dispensable for dimerization. *J. Struct. Biol.* **175**, 362–371 (2011).
36. J. J. Smith, J. D. Aitchison, Peroxisomes take shape. *Nat. Rev. Mol. Cell Biol.* **14**, 803–817 (2013).
37. V. Tillander, S. E. H. Alexson, D. E. Cohen, Deactivating fatty acids: Acyl-CoA thioesterase-mediated control of lipid metabolism. *Trends Endocrinol. Metab.* **28**, 473–484 (2017).
38. A. Shah, V. de Biasi, P. Camilleri, Development of a spectrophotometric method for the measurement of thiols at trace levels. *Anal. Proc.* **32**, 149–153 (1995).
39. J. K. Hiltunen *et al*., The biochemistry of peroxisomal beta-oxidation in the yeast *Saccharomyces cerevisiae*. *FEMS Microbiol. Rev.* **27**, 35–64 (2003).
40. W. H. Meijer *et al*., Peroxisomes are required for efficient penicillin biosynthesis in *Penicillium chrysogenum*. *Appl. Environ. Microbiol.* **76**, 5702–5709 (2010).
41. F. Hullin-Matsuda, T. Taguchi, P. Greimel, T. Kobayashi, Lipid compartmentalization in the endosome system. *Semin. Cell Dev. Biol.* **31**, 48–56 (2014).
42. D. Tholl, "Biosynthesis and biological functions of terpenoids in plants" in *Biotechnology of Isoprenoids*, J. Schrader, J. Bohlmann, Eds. (Advances in Biochemical Engineering/Biotechnology, Springer, Cham, 2015), pp. 63–106.
43. M. E. Elshobary *et al*., Tissue-specific localization of polyketide synthase and other associated genes in the lichen, *Cladonia rangiferina*, using laser microdissection. *Phytochemistry* **156**, 142–150 (2018).